Metals and Materials International (2023) 29:2018–2027
https://doi.org/10.1007/s12540-022-01352-z

Effect of Niobium on the Thermal Stability and Mechanical Properties of a Low-Carbon Ultrafine Grain Steel

Qingxiao Zhang[1] · Wei Wang[2] · Qing Yuan[1,3] · Zhoutou Wang[1] · Zhicheng Zhang[3] · Guang Xu[1]

Received: 22 September 2022 / Accepted: 14 November 2022 / Published online: 30 December 2022

Abstract

The effects of niobium (Nb) on the thermal stability and mechanical properties of a low-carbon ultrafine grain steel (UFG) were investigated. Results indicate that compared to the Nb-free UFG steel, the dissolved Nb in the Nb-UFG steel before annealing was beneficial to improve the thermal stability and strength but harmful to plasticity. The grain boundaries movement was inhibited by numerous Nb(C, N) particles re-precipitated during annealing, leading to the refined ferrite grains, subsequently the higher thermal stability and strength of the Nb-UFG steel. The decreased elongation was attributed to the finer ferrite grains and coarse Fe_3C particles. However, the thermal stability and strength of the Nb-UFG steel were also enhanced without any elongation sacrifice when Nb was partially dissolved in matrix before annealing. The superior balance between strength and ductility is ascribed to the precipitation strengthening of fine Nb(C, N) particles, appropriate ferrite grain size and finer Fe_3C particles. In addition, although the thermal stability of the steel with completely solute Nb before annealing was better than that with partially solute Nb, the strength and elongation of the former decreased due to the inferior work hardening ability caused by finer ferrite grains and larger Fe_3C particles.

Keywords Niobium · Ultra-fine grains · Precipitates · Thermal stability · Mechanical properties

1 Introduction

Low-carbon ultra-fine grain (UFG) steel manifests significant potential to replace high-strength alloyed steels due to its simple chemical composition. The UFG steels are mainly fabricated by severe plastic deformation (SPD) and thermo-mechanical controlled process (TMCP) [1–3]. Tsuji et al. first proposed a new method to fabricate the UFG steel by cold rolling martensite initial microstructure followed by annealing [4], which is easy to implement industrially in widely available steel production lines. After that, the UFG steels fabricated by different rolling temperatures and annealing routes were reported [5, 6]. In addition, different initial microstructures such as martensite + ferrite, pearlite + ferrite and bainite are used to fabricate the UFG steels [7–10]. For example, Wang et al. [7] fabricated the UFG steel with bimodal grain size to improve the ductility of UFG steels using initial structure of martensite and ferrite. Hosseini et al. [8] reported the improvement of plasticity in an UFG steel via high temperature short time annealing, which can be attributed to the formation of a bimodal grain size distribution and the precipitation of the secondary phases (cementite particles) within coarse grains. In addition, the ultra-fine grains of 700 nm were obtained by cold rolling and annealing with bainite initial structure [9].

The poor plasticity and thermal stability have been the concomitant drawbacks of high-strength UFG steels [11–13]. Many studies have been conducted to improve the plasticity and thermal stability of ultra-fine grain steels, which has confirmed the improvement of plasticity and microstructure thermal stability of ultra-fine grain steels by introducing second phase particles [14–17]. However, there are few studies focusing on the effect of Nb on the thermal stability and mechanical properties of UFG steels. The

✉ Wei Wang
weiwang@baosteel.com

✉ Guang Xu
xuguang@wust.edu.cn

[1] The State Key Laboratory of Refractories and Metallurgy, Key Laboratory for Ferrous Metallurgy and Resources Utilization of Ministry of Education, Wuhan University of Science and Technology, 430081 Wuhan, China

[2] Central Research Institute of Baoshan Iron and Steel Co., Ltd, 201900 Shanghai, China

[3] Daye Special Steel Co., Ltd, 435100 Daye, China

Table 1 Chemical composition of steels used in the present work (wt%)

Steel	C	Si	Mn	Nb	P	S	N	Fe
Nb-bearing	0.165	0.211	0.448	0.028	0.013	0.013	0.0028	Balance
Nb-free	0.164	0.213	0.450	–	0.014	0.013	0.0029	Balance

authors' previous studies proved that the thermal stability and mechanical properties of a UFG steel were improved by Nb(C, N) particles [18, 19]. However, the effects of austenitizing temperature, in other words, the solid solution state of Nb in austenite after austenization, on the thermal stability and mechanical properties of UFG steels were not considered in previous studies.

Therefore, in the present study, the effects of solid solution state of Nb after austenization or before annealing on the thermal stability and mechanical properties of a low-carbon UFG steel were investigated using a Nb-free UFG steel and a Nb-UFG steel by microstructure observation, precipitate analysis and mechanical test etc.

2 Materials and Experimental Procedure

The experimental steels with chemical compositions in Table 1 were used in the present investigation. Two steels were refined in a 50 kg vacuum induction furnace and hot-rolled to a 14 mm plate on a two-high mill. The rectangle specimens of 90 mm × 15 mm × 3 mm (length × width × thickness) were machined from hot-rolled plates. For Nb-steel, the specimens were respectively heated to two austenitizing temperatures (1050 and 1250 °C) for 30 min at a heating rate of 10 °C/s and then water-quenched to room temperature to obtain initial martensite microstructure. The specimens were labeled as the A1050 and A1250 specimens, respectively, according to the different austenitizing temperatures. In addition, the Nb-free specimens were heated to 1050 °C for 30 min and then water-quenched to room temperature. Afterwards, all quenched specimens were cold rolled from 3 mm to 1 mm on a two-high mill with a roll diameter of 310 mm with a total reduction of 65%. No cracks were found on the cold rolled specimens. The cold-rolled specimens were subsequently annealed at 400 ~ 600 °C for 30 ~ 60 min followed by air cooling to room temperature.

For the Nb-steel, carbon replicas were prepared to analyze the precipitates in the hot rolled, quenched and annealed specimens. Thin foils were prepared to observe the microstructure of the cold-rolled specimens using a JEM-2100 F transmission electron microscope (TEM) equipped with an energy-dispersive spectrometer (INCA-EDS) operating at 200 kV. In addition, the quenched and annealed specimens were first grounded and polished, and then etched for microstructural characterization. The microstructure was observed on cross section using a Nova Nano 400 field-emission scanning electron microscope (FE-SEM) equipped with an electron backscatter diffraction (EBSD) with the step size of 0.1 μm. The mechanical properties along the rolling direction of annealed specimens were measured using an Instron-3382 electronic universal tensile testing machine at a loading speed of 1 mm/min. The gauge size of all tensile specimens was 1.2 mm (thickness) ×2 mm (width) × 12 mm (length) with gauge length of 6 mm. Duplicate tests were conducted to improve the accuracy of mechanical properties. The hardness of the Nb-free and Nb-steels was measured using a Vickers hardness tester with a loading force of 300 g and a loading time of 10 s.

3 Results and Discussion

3.1 Microstructure

Figure 1 presents the TEM morphology of precipitates in the original (hot-rolled) and quenched specimens of A1250 and A1050 for the Nb-steel. The Nb-steel was alloyed with 0.028 wt% Nb and Nb precipitated as Nb(C, N) particles during solidification, rolling and coiling process after rolling (Fig. 1a). The black precipitates indicated by arrows were identified as Nb(C, N) particles by EDS analysis (Fig. 1b). It is observed that the precipitates are hardly observed in the A1250 specimen (Fig. 1c), while the A1050 specimen contains many precipitates (Fig. 1d), which means that Nb was almost completely dissolved in austenite matrix at 1250 °C and Nb was partially dissolved at 1050 °C.

The following formula for solid solubility product [20] is used to calculate the dissolution of Nb precipitates:

$$Log10[Nb][C + 12/14N] = \frac{-6770}{T} + 2.26 \quad (1)$$

where T is the temperature, K; *[Nb]* is the solid solution amount of Nb, wt%; *[C]* and *[N]* are the carbon and nitrogen contents in the experimental steel, wt%. The amount of solute Nb at 1050 °C was calculated to be 0.009%, so only partial precipitates were dissolved in the quenched A1050 specimen. In addition, the complete dissolution temperature of Nb(C, N) particles was estimated to be ~ 1202 °C. Therefore, Nb was almost completely dissolved in the quenched A1250 specimen as shown in the TEM observation in Fig. 1c, while the precipitates existed in the A1050 specimen because of partially dissolution of Nb (Fig. 1d).

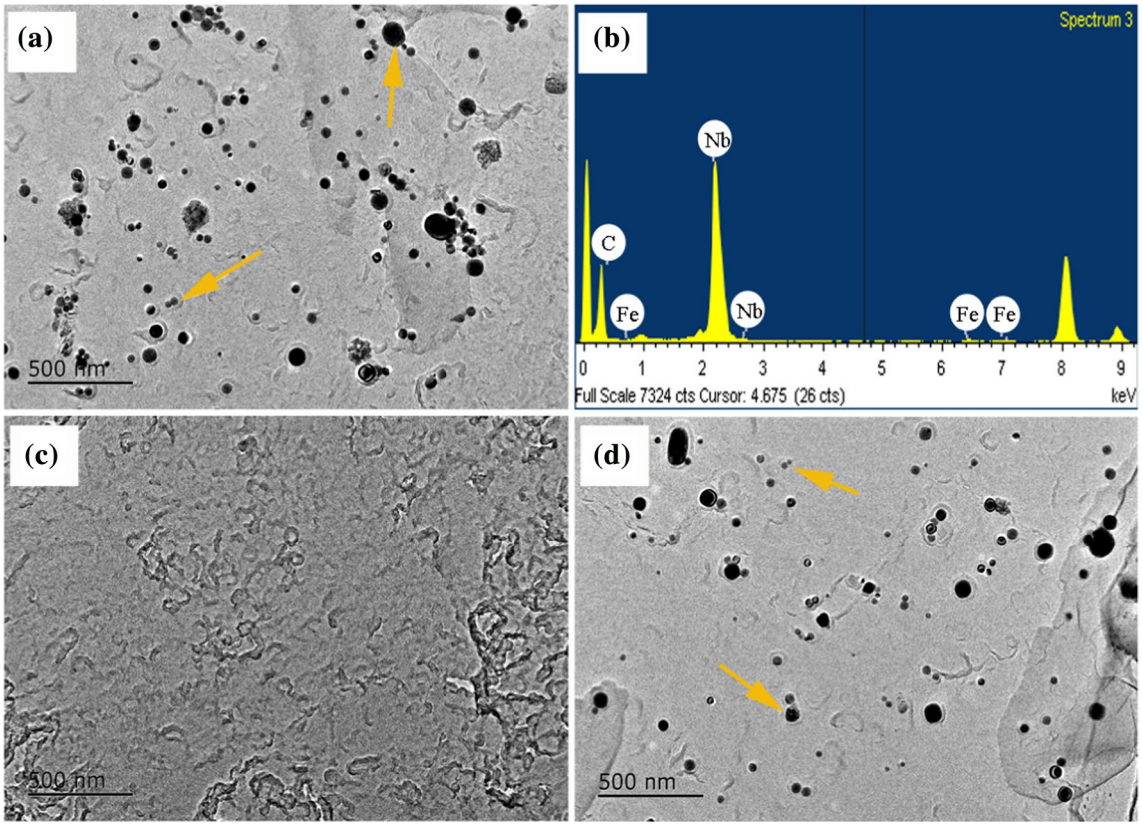

Fig. 1 TEM of precipitates of the: **a** hot-rolled specimen; and **b** the corresponding EDS result; **c** A1250 and **d** A1050 specimens after quenching

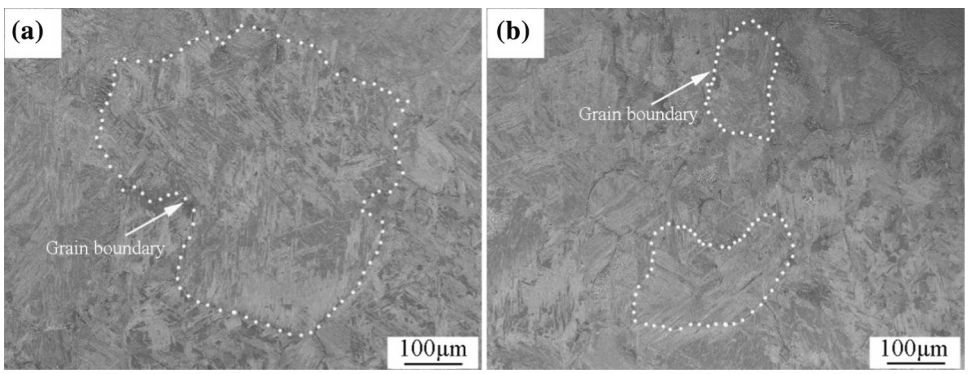

Fig. 2 The SEM microstructures of the **a** A1250 and **b** A1050 specimens after quenching

Typical SEM micrographs of the samples treated by different austenitizing temperatures are shown in Fig. 2. The microstructure of two samples is basically composed of martensite. In addition, the austenite grain size increases with the increased austenitizing temperature. Figure 3 displays the deformed martensite microstructure of the A1250 and A1050 specimens. It is observed that massive dislocations were generated by martensitic transformation and subsequent cold rolling. Martensitic transformation produces a large number of initial dislocations. Most of these initial dislocations are non-slip coordinated dislocations, and their Berger vector is difficult to be parallel to the Berger vector of movable dislocations formed in the deformation process. Hence, the dynamic recovery during cold rolling is suppressed. In addition, the nonequilibrium vacancies formed during quenching and cold rolling as well as the deformation heat generated during cold rolling promote the climbing of dislocations, which is conducive to the formation of dislocation cells. Moreover, the dislocation movement is hindered by the martensite laths, the interface between laths and original austenite grain boundaries, which further accelerates the dislocation accumulation. Therefore, the dislocation

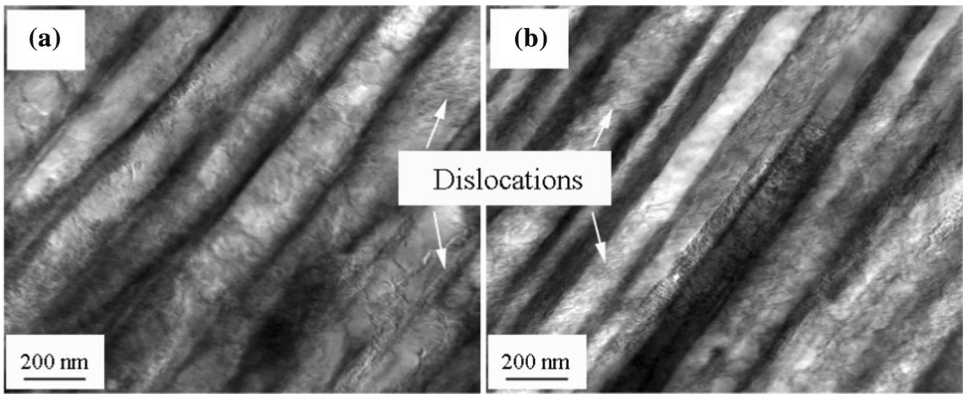

Fig. 3 Quenched and deformed martensite of the **a** A1250 and **b** A1050 specimens

density in martensite sharply increases after quenching and cold rolling [21].

The mean width of martensitic laths in the A1250 and A1050 specimens was measured to be 240 ± 25 and 182 ± 10 nm, respectively, indicating that the martensitic lath size was larger at high austenitizing temperature. For the Nb-steel, the martensite lath size is correlated with the austenite grain size, which is directly proportional to the austenitizing temperature and precipitate size, and inversely proportional to the volume fraction of precipitates [22]. On the one hand, the austenite grain size increases with the increased austenitizing temperature according to Arrhenius-type equations [23]. On the other hand, the precipitates were almost dissolved in matrix (Fig. 1c) at higher austenitizing temperature of 1250 °C, leading to less pining force. Thus, the martensite laths are coarsened at higher austenitizing temperature due to the larger austenite grains (Fig. 2), which is consistent with the results of Dong et al. [24].

The inverse pole figures (IPFs) of the A1250 and A1050 specimens are presented in Fig. 4. The pixel pairs exceeding the misorientation angle of 2° are recognized as grain boundaries. Low-angle grain boundarie (LAGBs 2–15°) are plotted by grey color, whereas high-angle grain boundaries (HAGBs ≧ 15°) are presented in black lines. Moreover, Ueji et al. [25] indicated that large portion of the boundaries surrounding the recrystallized equiaxed ultrafine ferrite grains are HAGBs. Hence, the HAGBs are considered in the grain size measurement. About 80–120 ferrite grains for each specimen were used to measure the mean size based on equivalent circle diameter method. Figure 5 shows the changes in grain size of the A1250 and A1050 annealed specimens. The mean size of ferrite grains in the A1250 specimen annealed at 500 °C for 60 min was measured to be 381 ± 21 nm (Fig. 4a), while the average grain size decreased to 245 ± 32 nm with the increasing of annealing temperature from 500–550 °C (Fig. 4c). The decrease of grain size at 550 °C may result from the re-precipitation of Nb(C, N) particles during annealing. The TEM morphologies of precipitates in the annealed specimens are presented in Fig. 6. It is observed that the Nb(C, N) particles are barely observed in the A1250 specimen annealed at 500 °C for 60 min (Fig. 6a), while many Nb(C, N) particles appear in the A1250 specimen at the annealing temperature of 550 °C (Fig. 6c). On the one hand, the recovery is suppressed because the movement of dislocations is restrained by numerous Nb(C, N) particles [25]. On the other hand, the grain growth is constrained because the migration of grain boundaries is also inhibited by Nb(C, N) particles [18]. Therefore, the mean size of ferrite grains obviously decreased with increasing annealing temperature from 500 to 550 °C. Moreover, the average size of ferrite grains in the A1250 specimen annealed at 600 °C for 30 min was measured to be 260 ± 41 nm (Fig. 4e), and no obvious further grain growth is observed in the A1250 specimen annealed at 600 °C for the prolonged annealing time of 60 min (285 ± 36 nm, Fig. 4g), demonstrating an excellent thermal stability of the A1250 specimen, which can also be attributed to the inhibited migration of grain boundaries by numerous Nb(C, N) particles.

The mean size of ferrite grains in the A1050 specimen annealed at 500 °C for 60 min was measured to be 351 ± 19 nm (Fig. 4b), which is finer than that of the A1250 specimen annealed at 500 °C for 60 min (381 ± 21 nm). This may result from the structure heredity. As can be seen in Fig. 3, the width of deformed martensite in the A1050 specimen is finer than that of the A1250 specimen. Besides, the migration of grain boundaries was inhibited by the fine Nb(C, N) particles retained from hot-rolled sheet in the A1050 specimen. Moreover, the average size of ferrite grains is slightly larger with increasing annealing temperature to 550 °C (365 ± 35 nm, Fig. 4d). The grain coarsening can be explained by distribution of Nb(C, N) particles. Although the fine Nb(C, N) particles (< 20 nm, Fig. 6d) retained from hot-rolled sheet and re-precipitated during annealing are conductive to grain refinement, the amount of fine Nb(C, N) particles in the A1050 specimen is limited due to the undissolved large Nb(C, N) particles (> 100 nm, Fig. 6b) [27]. Besides, the large Nb(C, N) particles (> 100 nm, Fig. 6a) cannot retard but accelerate the ferrite recrystallization

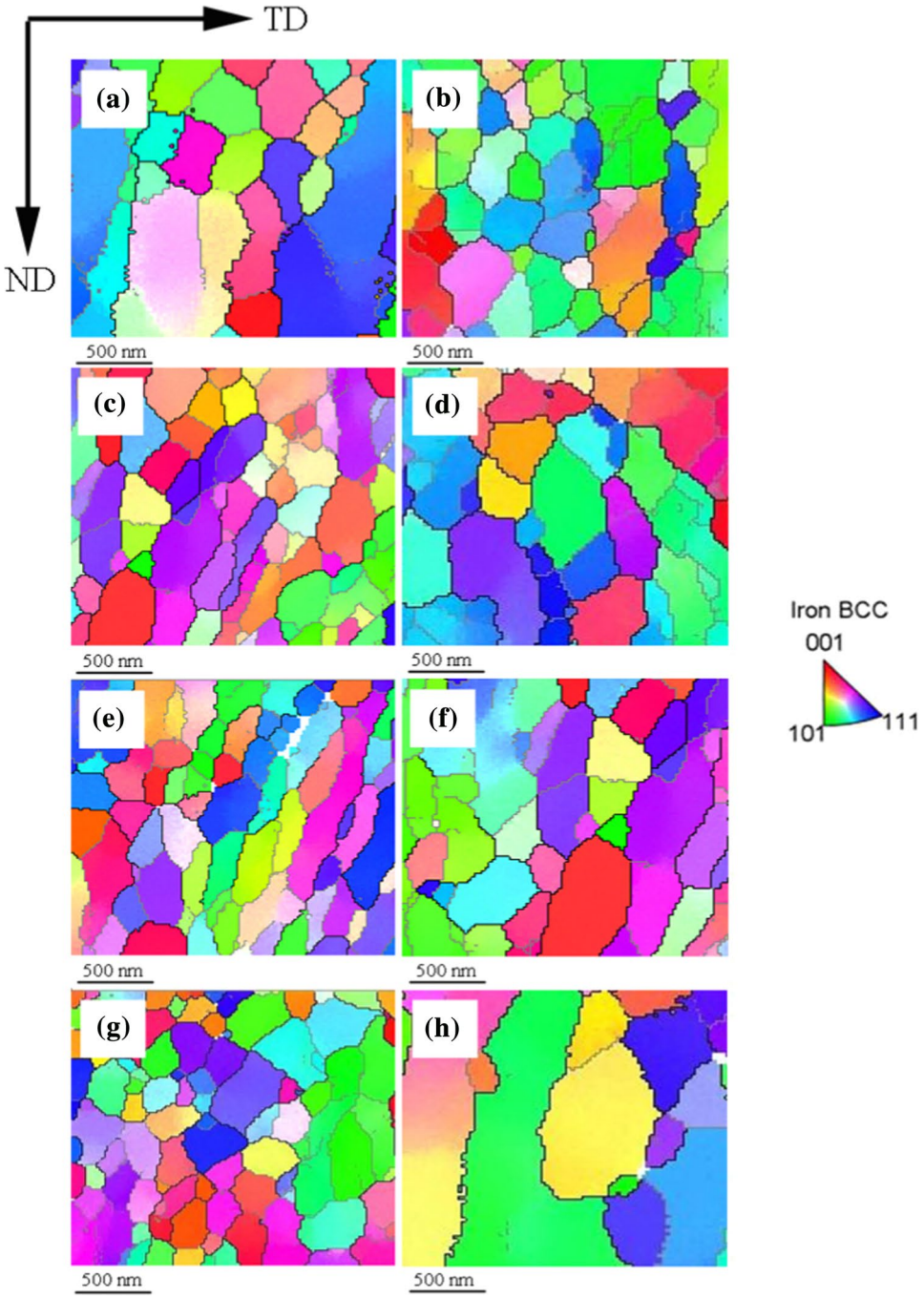

Fig. 4 Inverse pole figures of the selected specimens: the A1250 specimens annealed at **a** 500 °C for 60 min; **c** 550 °C for 60 min; **e** 600 °C for 30 min; **g** 600 °C for 60 min, and the A1050 specimens annealed at **b** 500 °C for 60 min; **d** 550 °C for 60 min; **f** 600 °C for 30 min; and **h** 600 °C for 60 min

because the nucleation of recrystallization is accelerated by heterogeneous deformation caused by large particles, which is known as particle stimulated nucleation of recrystallization (PSN) [28]. Hence, the grain refinement effect by the fine Nb(C, N) particles is overshadowed by grain coarsening due to large Nb(C, N) particles and increasing annealing temperature, thus leading to the slightly coarsened ferrite grains in the A1050 at 550 °C for 60 min. In addition, the ferrite grains in the A1050 specimen annealed at 600 °C for 60 min grew further (Fig. 4h). Therefore, compared to the A1250 specimen, the thermal stability of the A1050 specimen is worse, which can be explained by the limited pining effect of fine Nb(C, N) particles in the A1050 specimen. As shown in Fig. 6c, d, there are fewer re-precipitated fine particles during annealing in the A1050 specimen due to less Nb in solid solution state at the lower austenitizing temperature of 1050 °C. Gao et al. [29] used the phase field method to simulate the effect of precipitation particles on growth of grains and reported that the pinning effect of the Zener particles on the grain boundary was enhanced due

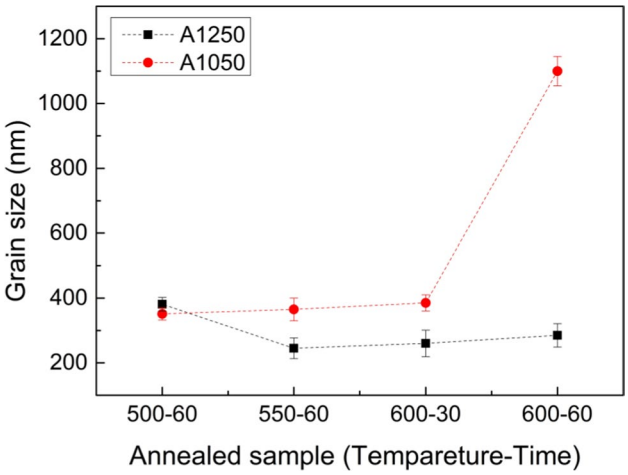

Fig. 5 Changes in grain size of the annealed samples in Nb-UFG steels

to the increased volume fraction of particles, leading to the decrease of grain growth rate and the maximum grain size. In addition, the number of particles increases with the decreased particle size because the volume fraction of Nb atoms is constant, leading to the better pinning effect. Hence, the thermal stability of the A1250 specimen is better. Moreover, the fractions of HAGBs of A1050 (65.4%, 72.8%, 78.5% and 89.6%, respectively) are higher than those of A1250 (corresponding to 62.3%, 63.5%, 70.2% and 75.9%, respectively) at different annealing conditions. The increased fraction of HAGBs in A1050 specimen indicates the declining thermal stability because the recrystallization nucleation is promoted with the HAGBs and the activation energy decreases as well.

3.2 Mechanical Property

Figure 7 shows the Vickers hardness as a function of annealing temperature and time. The decrease of hardness before 450 °C probably corresponds to the recovery, while the obvious softening from 450 to 500 °C corresponds to the recrystallization of ferrite grains. In addition, the hardness of the A1250 specimen slightly increases with the increasing of annealing temperature from 500 to 550 °C due to the grain refinement and re-precipitation of Nb(C, N), while the hardness of the A1050 specimen changes little with the increasing of annealing temperature from 500–550 °C due to the combined effect of temperature increase and re-precipitated particles of Nb(C, N). But in the case of the Nb-free UFG steel, more decrease of hardness is recognized. The results demonstrate that the thermal stability of Nb-steel is substantially enhanced. It is known that the Nb(C, N) particles strongly inhibits the grain growth and migration of grain boundaries at higher annealing temperature or longer time [18]. Hence, the enhanced thermal stability of Nb-steel is attributed to the re-precipitation of Nb(C, N) particles during annealing (A1250), or the fine Nb(C, N) particles retained from hot sheet and re-precipitated during annealing (A1050). In addition, hardness change of the A1250 specimen is very small with prolonged annealing time from 30 to 60 min at 600 °C, while the obviously softening is observed in the A1050 specimen, demonstrating a better thermal stability of the former than the later. This is because the pining effect of Nb(C, N) particles is limited due to relatively fewer fine Nb(C, N) particles re-precipitated during annealing in the A1050 specimen (Fig. 5c, d).

The mechanical properties of the A1250 and A1050 specimens after annealing are shown in Table 2. The optimum balance between the tensile strength (860.4 MPa) and elongation (15.55%) was obtained in authors' previous study for the Nb-free UFG steel annealed at 550 °C for 30 min [19]. The best mechanical properties of the A1050 and A1250 specimens were obtained after annealing at 550 °C for 60 min. The engineering strain-stress curves of the A1050 and A1250 specimens annealed at 550 °C for 60 min as well as the Nb-free UFG steel annealed at 550 °C for 30 min are exhibited in Fig. 8. The tensile strength of the A1050 specimen annealed at 550 °C for 60 min is 980.6 MPa and the elongation (15.45%) is almost the same as that of the Nb-free UFG steel. The increased strength is attributed to the precipitation strengthening by Nb(C, N) particles, and the similar elongation can be explained by the similar size of ferrite grains between the A1050 specimen and Nb-free UFG steel. In addition, Yang et al. [30] reveled that nanoprecipitates not only hinder the dislocation glide but also promote the multiplication of dislocations. In other words, the nanoprecipitates simultaneously serve as obstacles of dislocation movement and sources of dislocation accumulation, resulting in dislocation strengthening, which is consistent with the results of our previous study [19]. For the A1250 specimen, the tensile strength annealed at 550 °C for 60 min reaches 950.2 MPa, but its elongation is smaller (10.34%). In comparison to the Nb-free UFG steel, the increased strength is ascribed to the grain refinement and precipitation strengthening, while the decreased elongation is probably attributed to the smaller ferrite grain size. Moreover, the similar mechanical properties were obtained in the A1250 specimens annealed at 550 and 600 °C due to the similar grain size (Fig. 5). Furthermore, the properties of the A1050 specimen annealed at 550 °C for 60 min have no significant change compared with that annealed at 600 °C for 30 min, which can also be ascribed to the similar grain size (Fig. 5). However, the strength sharply decreases in the A1050 specimen annealed at 600 °C for 60 min due to the coarsening of ferrite grains (Fig. 5).

Based on the Hall-Petch relationship, the yield strength increases with the decrease of ferrite grain size. As shown in

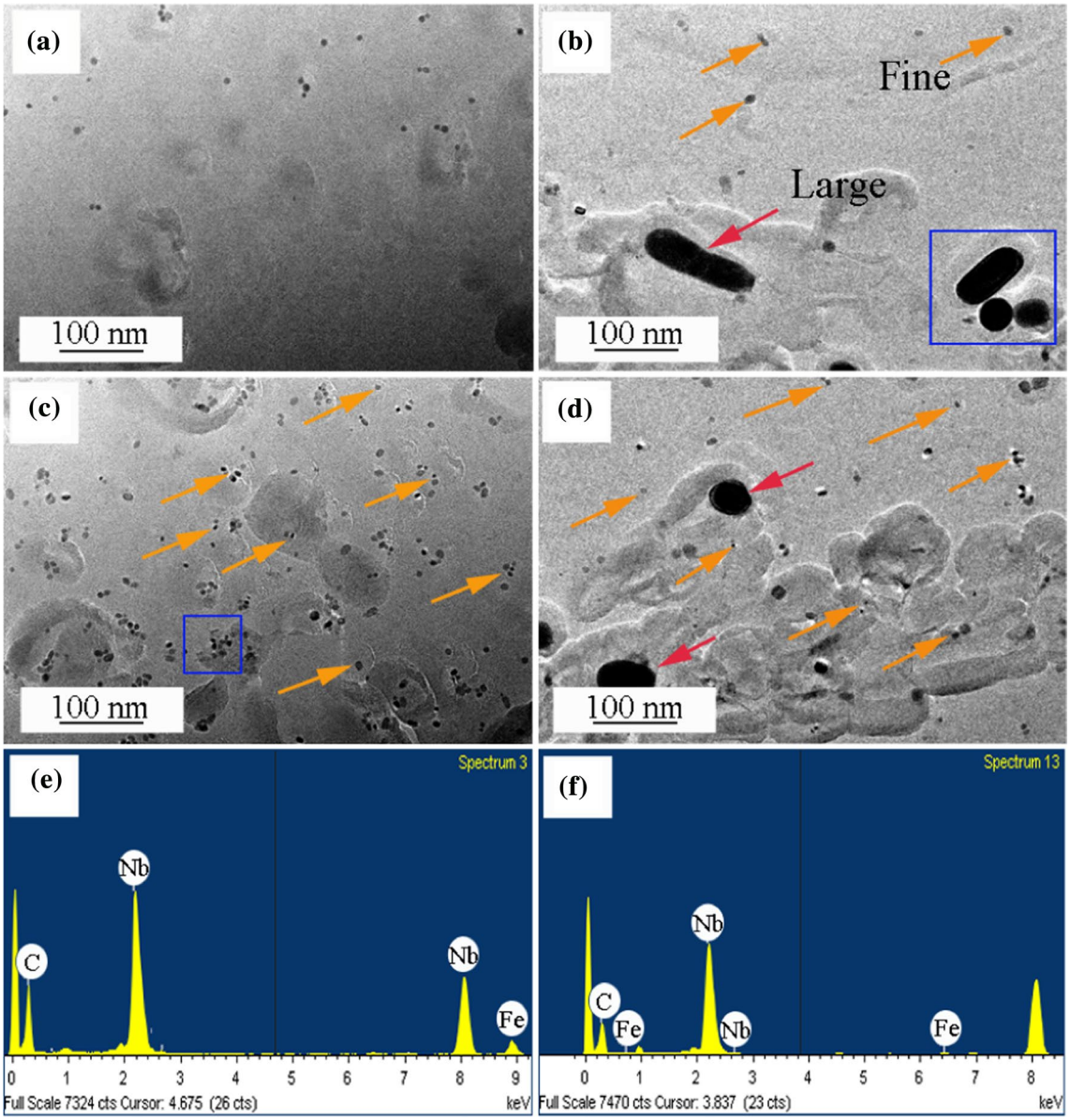

Fig. 6 TEM of precipitates of the **a** A1250 specimen annealed at 500 °C for 60 min; **b** A1050 specimen annealed at 500 °C for 60 min; **c** A1250 specimen annealed at 550 °C for 60 min; **d** A1050 specimen annealed at 550 °C for 60 min; **e** the corresponding EDS results of fine particles in box of c and **f** the corresponding EDS results of large particle marked in box of b

Fig. 8, in comparison to the A1050 specimen, the increased yield strength of the A1250 specimen is ascribed to the finer grains (Fig. 4) and more Nb(C, N) particles (Fig. 6). However, the tensile strength and total elongation of the A1250 specimen are smaller than those of the A1050 specimen. This can be explained by the ferrite grain size and the distribution of Fe_3C particles. The SEM morphologies of Fe_3C particles in the A1050 and A1250 specimens annealed at 550 °C for 60 min are given in Fig. 9, where two types of Fe_3C particles, termed as intragranular and intergranular particles, are observed. The intergranular Fe_3C particles are larger than the intragranular particles. This is because the defects and alloy elements are easy to accumulate at grain boundaries. Besides, the free energy at grain boundaries is much higher than that within the grains, thus facilitating the coarsening of Fe_3C particle at grain boundaries. In comparison to the A1050 specimen, it is observed in Fig. 8 that the coarsening is very serious both for intragranular and intergranular particles in the A1250 specimen, especially the latter. It is well known that the diffusion rate of solute

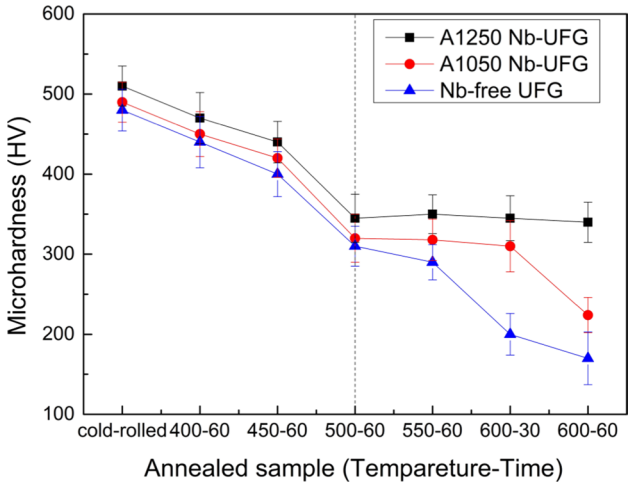

Fig. 7 Vickers hardness as a function of annealing temperature and time

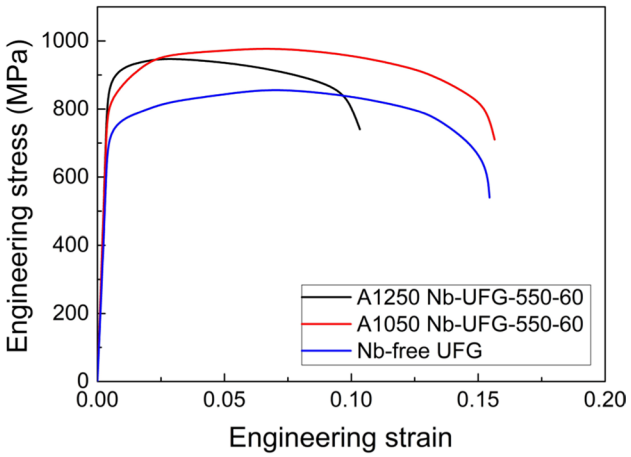

Fig. 8 Engineering strain-stress curves of the Nb-UFG and Nb-free UFG steels

Table 2 Mechanical properties of the A1050 and A1250 specimens after annealing

Specimen	Treatment	Tensile strength (MPa)	Elongation (%)
A1250	550 °C for 60 min	950.2	10.34
	600 °C for 30 min	945.5	10.28
	600 °C for 60 min	942.3	9.75
A1050	550 °C for 60 min	980.6	15.45
	600 °C for 30 min	965.8	15.13
	600 °C for 60 min	680.3	28.28
Nb-free steel	550 °C for 30 min	860.4	15.55

atoms at the grain boundary is significantly higher than that in the matrix [31]. Besides, solute atoms are more likely to segregate on grain boundaries. Hence, the grain boundaries provide fast paths for atomic diffusion, and the coarsening of Fe_3C particles in the A1250 specimen is attributed to larger diffusion coefficients of solute atoms (such as carbon atoms), which result from more amount grain boundaries due to smaller grains. In addition, the relationship between the mean diameter of Fe_3C particles ($\bar{r}$) and growing time (t) is expressed by Eq. (2) [32]:

$$\left(\bar{r}\right)^3 - r_0{}^3 = kt \tag{2}$$

where r_0 is the mean diameter of Fe_3C particles at the beginning of annealing process, k is a constant which is positively related with the diffusion coefficient D, interface energy γ and equilibrium solubility of large particles X_e as shown in Eq. (3):

$$k \propto D\gamma X_e \tag{3}$$

This indicates that the higher interface energy in the finer grains facilitates the growth of Fe_3C particles. Therefore, the larger Fe_3C particles were formed in the A1250 specimen due to smaller grains.

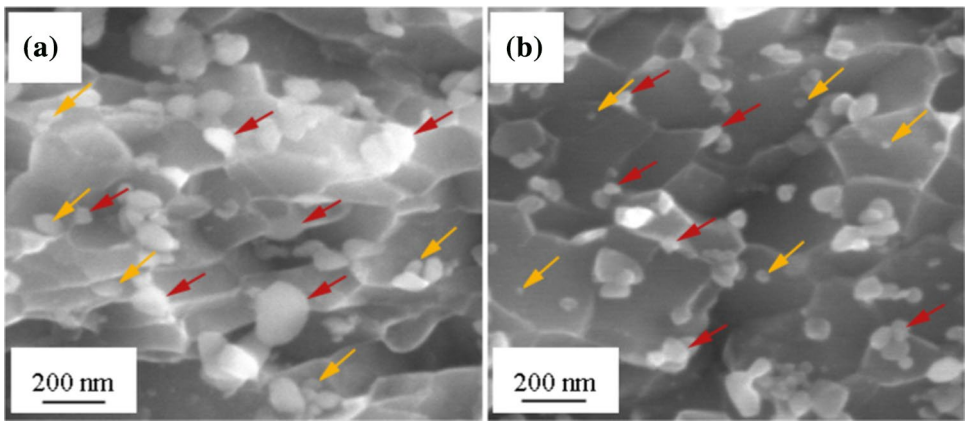

Fig. 9 The SEM morphologies of Fe_3C particles of the **a** A1250 and **b** A1050 specimens annealed at 550 °C for 60 min

It is well known that the work hardening of UFG steels is normally inferior compared with the coarse grain counterparts. On the one hand, the dislocation accommodation ability of UFG steels is insufficient. On the other hand, the grain boundary area in per unit volume of UFG steels increases, motivating the dynamic recovery and annihilation of neighboring dislocations during annealing [33]. The work hardening is not only related to ferrite grains, but also related to Fe_3C particles. The finer particles could guarantee the better work hardening due to the GNDs generation and accumulation [14]. Besides, the dislocation accommodation ability decreases with the decreased grain size. In addition, larger intergranular Fe_3C particles occupy the positions of fractional grain boundaries, deteriorating the strength of the grain boundaries. Therefore, in comparison to the A1050 specimen, the decreased strength and elongation of the A1250 specimen is ascribed to the inferior work hardening ability (Fig. 8) caused by the finer ferrite grains and larger Fe_3C particles.

4 Conclusion

The effects of solute Nb before annealing on the thermal stability and mechanical properties of low-carbon UFG steels were investigated. The following conclusions can be drawn:

(1) In comparison to the Nb-free UFG steel, the thermal stability is enhanced, and the strength of the Nb-UFG steel is improved and the elongation decreases when Nb is in complete solute state before annealing.
(2) In comparison to the Nb-free UFG steel, the strength and thermal stability of the Nb-UFG steel are greatly enhanced without sacrifice of its elongation when Nb is in partially solute state before annealing, and the main strengthening mechanisms are dislocation and precipitation strengthening.
(3) The thermal stability of Nb-UFG steel is better when Nb is in completely solute state before annealing than that Nb in partial solute state, whereas the strength and elongation of the former are worse than the latter due to the inferior work hardening ability caused by the finer ferrite grains and larger Fe_3C particles.

Acknowledgements This research was supported by the National Nature Science Foundation of China [Nos.52004193 and 51874216] and the China Postdoctoral Science Foundation [No.2022M710596].

Declarations

Conflict of interest The authors declare that they have no known competing financial interests or personal relationships that could have appeared to influence the work reported in this paper.

References

1. L.J. Zhao, N. Park, Y.Z. Tian, S. Chen, A. Shibata, N. Tsuji, Mater. Lett. **5**, 61 (2017)
2. M. Dao, L. Lu, R.J. Asaro, J.T.M. De Hosson, E. Ma, Acta Mater. **55**, 4041 (2007)
3. R. Song, D. Ponge, D. Raabe, J.G. Speer, D.K. Matlock, Mater. Sci. Eng. A **441**, 1 (2006)
4. N. Tsuji, R. Ueji, Y. Minamino, Y. Saito, Scripta Mater. **46**, 305 (2002)
5. Q. Yuan, G. Xu, S. Liu, M. Liu, H.J. Hu, G.Q. Li, Metals **8**, 518 (2018)
6. Q. Yuan, G. Xu, M. Liu, H.J. Hu, J.Y. Tian, Steel Res. Int. **90**, 1800318 (2019)
7. T.S. Wang, E. Zhang, M. Zhang, B. Lv, Mater. Sci. Eng. A **485**, 456 (2008)
8. S.M. Hosseini, M. Alishahi, A. Najafizadeh, A. Kermanpur, Mater. Lett. **74**, 206 (2012)
9. M. Hamzeh, A. Kermanpur, A. Najafizadeh, Mater. Sci. Eng. A **593**, 24 (2014)
10. H. Azizi-Alizamini, M. Militzer, W.J. Poole, Scripta Mater. **57**, 1065 (2007)
11. N. Tsuji, Y. Ito, Y. Saito, Y. Minamino, Scripta Mater. **47**, 893 (2002)
12. K.T. Park, Y.S. Kim, J.G. Lee, D.H. Shin, Mater. Sci. Eng. A **293**, 165 (2000)
13. K.T. Park, S.Y. Han, D.H. Shin, Y.K. Lee, K.J. Lee, K.S. Lee, ISIJ Int. **44**, 1057 (2004)
14. R. Song, D. Ponge, D. Raabe, Scripta Mater. **52**, 1075 (2005)
15. D. Raabe, D. Ponge, O. Dmitrieva, B. Sander, Scripta Mater. **60**, 1141 (2009)
16. J.C. Fisher, E.W. Hart, R.H. Pry, Acta Mater. **1**, 336 (1953)
17. Z. Li, T.S. Wang, X.J. Zhang, F.C. Zhang, Mater. Sci. Eng. A **552**, 204 (2012)
18. Q.X. Zhang, Q. Yuan, Z. Wang, W.W. Qiao, G. Xu, Steel Res. Int. **93**, 2100320 (2022)
19. Q.X. Zhang, Q. Yuan, Z. Wang, W.W. Qiao, G. Xu, Metall. Mater. Trans. A **52**, 5123 (2021)
20. A. Ghosh, S. Das, S. Chatterjee, B. Mishra, P. Ramachandra Rao, Mater. Sci. Eng. A **348**, 299 (2003)
21. S. Maropoulos, S. Karagiannis, N. Ridley, Mater. Sci. Eng. A **483–484**, 735 (2008)
22. Y. Okitsu, N. Takata, N. Tsuji, Scripta Mater. **60**, 76 (2009)
23. E. Anelli, ISIJ Int. **32**, 440 (1992)
24. J. Dong, C.X. Liu, Y.C. Liu, C. Li, Q.Y. Guo, H.J. Li, Mater. Sci. Forum **848**, 624 (2016)
25. R. Ueji, N. Tsuji, Y. Minamino, Y. Koizumi, Acta Mater. **50**, 4177 (2002)
26. T. Ogawa, N. Sugiura, N. Maruyama, N. Yoshinaga, Mater. Sci. Eng. A **564**, 42 (2013)
27. A.J Craven, K He, L.A.J Garvie, T.N Baker, Acta Mater. **48**, 3857 (2000)
28. H. Miura, T. Sakai, A. Belyakov, G. Gottstein, M. Crumbach, J. Verhasselt, Acta Mater. **51**, 1507 (2003)
29. Y.J. Gao, H.L. Zhang, X. Jin, C.G. Huang, Z.R. Luo, Acta Metall. Sin. **45**, 1190 (2009)
30. H. Yang, K. Li, Y. Bu, J. Wu, Y. Fang, L. Meng, J. Liu, H. Wang, Scripta Mater. **195**, 113741 (2021)
31. Q.L. Yong, *The Second Phase in Iron and Steel*, vol. 5 (Metallurgical Industry Press, Beijing, 2006)
32. J.S. Pan, J.M. Tong, M.B. Tian, *Fundamentals of Materials Science* (Tsinghua Humanities Press, Beijing, 2004), p. 589
33. R. Sandstrm, Acta Metall. **25**, 897 (1977)